Interplay of electronic and geometry shell effects in properties of neutral and charged Sr clusters

Andrey Lyalin,[1,2,*] Ilia A. Solov'yov,[1] Andrey V. Solov'yov,[1,†] and Walter Greiner[1]
[1]*Frankfurt Institute for Advanced Studies, Johann Wolfgang Goethe-University, Max-von-Laue Str. 1, 60438 Frankfurt am Main, Germany*
[2]*Imperial College of London, The Blackett Laboratory, Prince Consort Road, London SW7 2BW, United Kingdom*
(Received 1 March 2007; revised manuscript received 3 April 2007; published 14 May 2007)

The optimized structure and electronic properties of neutral, singly, and doubly charged strontium clusters have been investigated using *ab initio* theoretical methods based on density-functional theory. We have systematically calculated the optimized geometries of neutral, singly, and doubly charged strontium clusters consisting of up to 14 atoms, average bonding distances, electronic shell closures, binding energies per atom, the gap between the highest occupied and the lowest unoccupied molecular orbitals, and spectra of the density of electronic states (DOS). It is demonstrated that the size evolution of structural and electronic properties of strontium clusters is governed by an interplay of the electronic and geometry shell closures. Influence of the electronic shell effects on structural rearrangements can lead to violation of the icosahedral growth motif of strontium clusters. It is shown that the excessive charge essentially affects the optimized geometry of strontium clusters. Ionization of small strontium clusters results in the alteration of the magic numbers. The strong dependence of the DOS spectra on details of ionic structure allows one to perform a reliable geometry identification of strontium clusters.

DOI: 10.1103/PhysRevA.75.053201 PACS number(s): 36.40.Cg, 36.40.Mr, 31.10.+z, 31.15.Ne

I. INTRODUCTION

During the past two decades numerous theoretical and experimental works have been devoted to the study of stability, ionic structure, and electronic properties of metal clusters. Comprehensive survey of the field can be found in review papers and books; see, e.g., [1–12].

The most explored type of metal clusters are the clusters of the alkali metals. It is worth mentioning that the electronic shell structure of metal clusters has been discovered by the observation of the strong peaks in the mass spectra of sodium clusters [13]. The enhanced stability of some clusters, the so-called magic clusters, has been explained by the closure of shells of delocalized electrons. A simple physical model describing the electronic shell structure of metal clusters has been developed within the jellium approximation (see, e.g., [6,15,16]) by analogy with the shell model of atomic nuclei (see, e.g., [14]).

The jellium model is very successful for the simple alkali metals, for which one electron per atom is delocalized, see, e.g., [1,2,15–23] and references therein. The jellium model electronic shell closures for alkali metal clusters define the magic numbers $N=8$, 20, 34, 40, 58, and 92 that are in good agreement with experiment. However, clusters of alkali metals are not representative for the whole class of metal clusters. Clusters of alkaline-earth metals of the second group of the Periodic Table are expected to differ from the jellium model predictions at least at small cluster sizes. In this case, bonding between atoms is expected to have some features of the van der Waals type of bonding, because the electronic shells in the divalent atoms are filled. Therefore, the evolution of the alkaline-earth metal cluster properties is governed by an interplay of the electronic and geometry shell closures. That fact implies using direct *ab initio* molecular dynamics simulations methods rather than simple jellium model approaches when exploring electronic properties and structure of alkaline-earth metal clusters. The structural behavior of alkaline-earth metals is peculiar. With increasing atomic number, the crystalline structure of the bulk alkaline-earth metals alters from hexagonal closed packed (hcp) for Be and Mg to faced centered cubic (fcc) for Ca and Sr and finally to body centered cubic (bcc) for Ba [24]. Thus clusters of alkaline-earth metals are very appropriate to study structural transformations, nonmetal to metal transition, testing different theoretical methodologies, and conceptual developments of atomic cluster physics. However, relatively little work has been done so far on the exploration of the alkaline-earth metal clusters in comparison with that for the alkali metal clusters; see, e.g., [6,25] and references therein.

Among clusters of the alkaline-earth metals the most significant attention was paid to the berillium and magnesium clusters; see, e.g., [12,26–35] and references therein. The geometrical structure and bonding nature of Mg_N clusters with N up to 13 have been studied in [29] using the density-functional molecular-dynamics method. The size evolution of bonding in magnesium clusters Mg_N with $N=8-13$, 16, and 20 have been studied in [33] using the local-density approximation that accounts for gradient corrections. Structural and electronic properties of small magnesium clusters ($N\leqslant 13$) were studied in [30] using a first-principles simulation method in conjunction with the density-functional theory (DFT) and the generalized gradient correction approximation for the exchange-correlation functional. It was shown [30] that the metallization in magnesium clusters has a slow and nonmonotonic evolution, although, also jellium-

*On leave from Institute of Physics, St. Petersburg State University, Ulianovskaya str. 1, 198504 St. Petersburg, Petrodvorez, Russia. Email address: lyalin@fias.uni-frankfurt.de
†On leave from A. F. Ioffe Physical-Technical Institute, Polytechnicheskaya 26, 194021 St. Petersburg, Russia.

type magic clusters were observed [29,33]. In order to extend such calculations to larger systems, symmetry restricted methods have been developed. The spherically averaged–pseudopotential scheme with the local and nonlocal pseudopotentials has been used for the investigation of the electronic structure and shell closures of spherical Mg_N clusters up to $N=46$ [36]. Various properties of magnesium clusters, such as their structure and formation of the basic elements of the hcp lattice, the binding energy, ionization potentials, energy gap between the highest occupied and the lowest unoccupied molecular orbitals (HOMO-LUMO gap), average distances, and their evolution with the cluster size have been investigated theoretically (see [26–28] and references therein). All-electron DFT calculations of the energetic and structural properties of neutral magnesium clusters Mg_N ($N=2$ to 22 and selected clusters up to 309) have been performed in [64]. The mass spectrum of magnesium clusters was recorded [37,38] and the sequence of magic numbers was determined.

Not many works have been devoted to strontium clusters. Initially the structures and stability of strontium clusters with the number of atoms N up to 20 have been investigated using an empirical atomistic potential of the Murrell-Mottram type [39]. The pairwise additive Morse potential has been utilized in Ref. [40]. Both of these potentials have been used to predict properties of bulk strontium and can also be employed to describe strontium clusters. In the case of the Morse potential, clusters with polytetrahedral components dominate the growth process [40], whereas in the case of the Murrell-Mottram potential, the icosahedral growth dominates, with local regions of enhanced stability at $N=4$, 7, 13, and 19 [39]. At the *ab initio* level, calculations have been performed within local-density approximation for the Sr_2 molecule [41] and small strontium clusters up to 13 atoms [42]. The *ab initio* molecular-dynamics method with a plane-wave basis and ultrasoft pseudopotentials have been used to study the evolution of electronic states and multishell relaxations in strontium clusters Sr_N with number of atoms $N=2-35$, 55 and 147 [43]. In Ref. [44] a many-body potential for strontium clusters has been developed with parameters fitted to the energy surface of strontium clusters containing up to 10 atoms calculated within the density-functional theory (DFT) in the generalized gradient approximation. Structure and energetics of the most stable cluster isomers with up to 63 atoms have been obtained with genetic algorithms [44]. It has been shown that the sequence of magic clusters possessing enhanced stability with respect to its neighboring sizes changes significantly with temperature [44]. This behavior is due to structural transitions of the strontium clusters that occur at finite temperatures. Experimentally obtained mass spectra of the strontium clusters show that the magic numbers are substantially different than those of Lennard-Jones clusters [44–46].

Stability and fission of the positively charged strontium clusters have been studied theoretically within a simple liquid-drop model [47] and experimentally [47–50]. It has been found experimentally that the internal thermal excitation can influence fission channels and promote Coulombic fission [48]. On the other hand, fission into two charged fragments can stimulate an additional ejection of a neutral atom during or immediately after the system overcomes the fission barrier. Such an interplay between the Coulombic fission and the evaporation processes has been observed recently in Ref. [50], and analyzed theoretically in Ref. [51]. Thermal promotion of Coulombic fission of the Sr_7^{2+} has been predicted [51]. Stability towards monomer evaporation and fission of small neutral and positively charged strontium clusters has been studied by means of *ab initio* DFT methods in Ref. [51].

In this paper we investigate the optimized ionic structure and the electronic properties of neutral, singly, and doubly charged strontium clusters within the size range $N \leqslant 14$. We calculate optimized geometries, average bonding distance, electronic shell closures, binding energies per atom, HOMO-LUMO gap, and spectra of the electronic density of states. We demonstrate that the size evolution of structural and electronic properties of strontium clusters is governed by an interplay of the electronic and geometry shell closures. We show that the influence of the electronic shell effects on structural rearrangements can lead to violation of the icosahedral growth motif of strontium clusters. We study how the excessive charge affects the optimized geometry and other properties of the strontium clusters and demonstrate that ionization of the small strontium clusters results in the alteration of the sequence of magic numbers. We demonstrate that the strong dependence of the density of electronic states (DOS) spectra on details of ionic structure allows one to perform a reliable identification of the geometry of strontium clusters. Our calculations are based on *ab initio* theoretical methods invoking the density-functional theory and molecular dynamics simulations. The results obtained are compared with the available experimental data and the results of other theoretical works.

The atomic system of units, $|e|=m_e=\hbar=1$, has been used throughout the paper, unless other units are indicated.

II. THEORETICAL METHODS

Our calculations are based on *ab initio* theoretical methods invoking the density-functional theory. The standard SDD $(6D,10F)$ basis set of primitive Gaussians has been used to expand the cluster orbitals formed by the $4s^24p^65s^2$ outer electrons of Sr (10 electrons per atom). The remaining 28 core electrons $1s^22s^22p^63s^23p^63d^{10}$ of the Sr atom are represented by a core-polarization potential (see, e.g., [52] and references therein). The computations are performed within the DFT method based on the hybrid Becke-type three-parameter exchange functional [53] paired with the gradient-corrected Perdew-Wang 91 correlation functional (B3PW91) [54,55]. Such an approach has proved to be a reliable tool for the *ab initio* level studying the structure and properties of strontium clusters [44].

The cluster geometries have been determined by finding local minima on the multidimensional potential energy surface. We have applied an efficient scheme of global optimization called the cluster fusion algorithm (CFA) [56–58]. The scheme has been designed within the context of determination of the most stable cluster geometries and it is applicable for various types of clusters [58]. We have used a

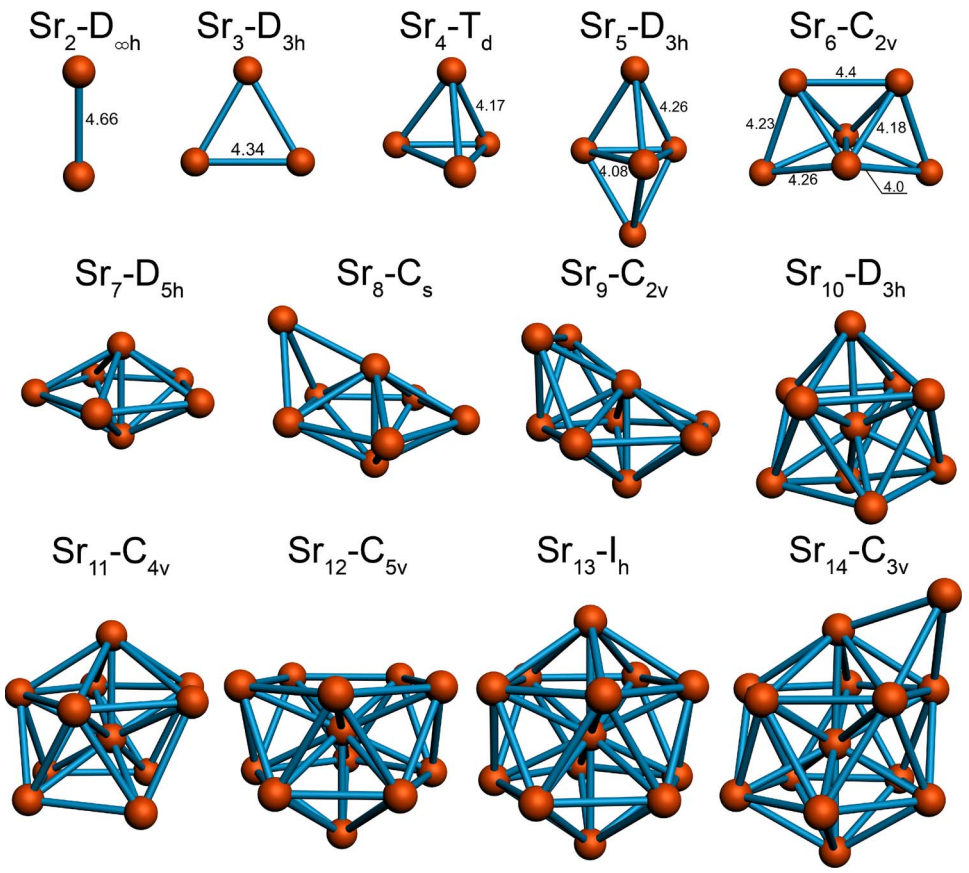

FIG. 1. (Color online) Optimized geometries of neutral strontium clusters Sr_2–Sr_{14} calculated in the B3PW91/SDD(6D,10F) approximation. The interatomic distances are given in angstroms. The label above each cluster image indicates the point symmetry group of the cluster.

similar approach to find the optimized geometries for noble gas clusters, and Na, Mg, and La metal clusters [25,26,56,59].

While the global energy optimization for noble gas clusters is a relatively simple problem and optimization could easily be done for larger clusters, the calculations with metal clusters present a serious challenge and require significant computational resources. For both types of calculations the CFA has proven to be a reliable and effective tool in multidimensional global optimization. The proposed algorithm belongs to the class of genetic (also called evolutionary) global optimization methods [60,61].

In applications to clusters the genetic methods are based on the idea that the larger clusters evolve to low energy states by mutation and/or by mating smaller structures with low potential energy. Our method uses the strategy of adding one atom to a cluster of size $N-1$. There are, however, two important improvements which allow for a much faster convergence in comparison with standard genetic methods. The first one is the fact that the atom is not added at a random place on the surface of the initial cluster. Rather, we use the deterministic approach and the new atom is added to certain places of the cluster surface, such as the midpoint of a face. The second important feature of our method is that we add the new atom not only to the ground state isomer of size $N-1$, but also to the other, energetically less favorable, isomers. This insures that we do not miss sizes at which smooth evolution within one family of clusters (say, with the same type of lattice) is interrupted and the global energy minimum of the next cluster size lies within another cluster growth branch.

Note that, during the optimization process, the geometry of the cluster as well as its initial symmetry sometimes change dramatically. All the characteristics of the clusters, which we have calculated and present in the following section, are obtained for the clusters with the optimized geometry. With increasing cluster size, such calculations become computer time demanding. In this work, we limit the calculations by the cluster size $N=14$. Calculations have been carried out with the use of the GAUSSIAN 03 software package [62].

III. NUMERICAL RESULTS AND DISCUSSION

A. Geometry optimization of Sr_N, Sr_N^+, and Sr_N^{2+} clusters

The results of the cluster geometry optimization for neutral, singly, and doubly charged strontium clusters consisting of up to 14 atoms are shown in Figs. 1–3, respectively.

Strontium clusters possess various isomer forms whose number grows dramatically with cluster size. In Figs. 1–3, we present the lowest energy configurations optimized with the B3PW91 functional. The interatomic distances are given in angstroms. The label above each cluster image indicates the point symmetry group of the cluster.

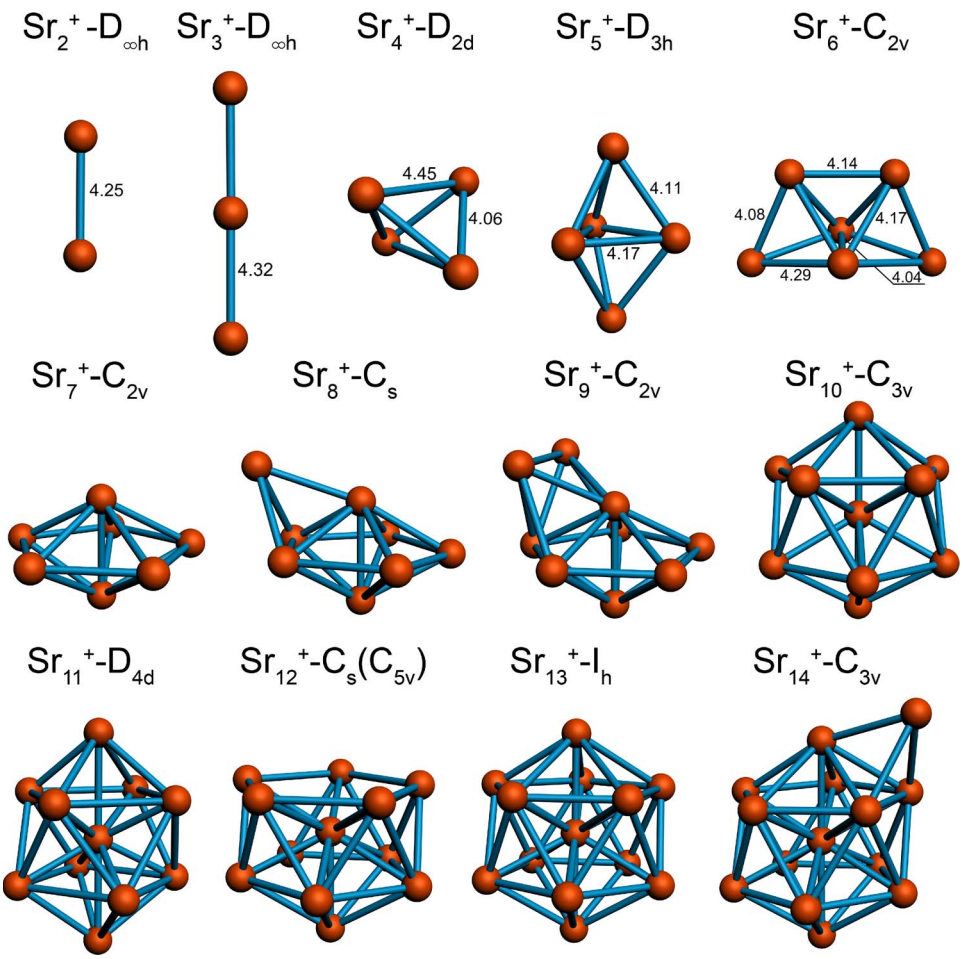

FIG. 2. (Color online) Same as in Fig. 1, but for singly charged strontium clusters Sr_2^+–Sr_{14}^+.

For the determination of symmetry of different clusters certain constraints were used. The interatomic distances and the angles were considered as equal within the tolerance of 0.07 Å and 1°, respectively. The constraints on the distances and on the angles roughly correspond to the error in the total energy of the system, which in our case is about 10^{-5} a.u. If the deviation of some distances (or angles) was greater than the chosen constraint value, and the cluster is topologically close to a structure with higher symmetry, we indicate the higher symmetry in the brackets (see Sr_{12}^+, Sr_{12}^{2+}, and Sr_{13}^{2+} in Figs. 2 and 3).

Figure 1 shows that neutral strontium clusters form the compact structures, maximizing the coordination number. The Sr_2 dimer is weakly bound possessing the dissociation energy 0.139 eV, the bond length 4.659 Å, and the harmonic vibrational frequency 45.33 cm^{-1}, which is in good agreement with the experimental results of Ref. [63], where the values 0.131 ± 0.004 eV for the dissociation energy, 4.45 Å for the bond length, and 40.32 ± 0.02 cm^{-1} for the vibrational frequency have been reported. The lowest energy state for Sr_3 is an equilateral triangle and for Sr_4 is a regular tetrahedron. As we discuss below, the Sr_4 cluster is relatively more stable and compact, as compared to the neighboring clusters. The Sr_5 cluster has a structure of slightly elongated triangular bipyramid. These structures are in good agreement with the results obtained with the use of the empirical potential of Murrell-Mottram type [39]. For larger strontium clusters, in particular with $N=6$, 9, and 10, we found that the lowest-energy isomers optimized within B3PW91/SDD($6D$,$10F$) DFT method are considerably different from the Murrell-Mottram structures. Although the Murrell-Mottram method reproduces most stable structures with the closed geometry shells it obviously fails to reproduce the influence of electronic shell effects on cluster geometry. The Sr_6 consists of three pyramids connected by their faces, Sr_7 is a pentagonal bipyramid, and Sr_8 is a capped pentagonal bipyramid. These geometrical structures are in good agreement with the results of Ref. [44]. For $N \leqslant 8$, the lowest-energy strontium isomers are the same as for magnesium clusters, see, e.g., Refs. [26–28,64]. Figure 1 demonstrates that the bonds between the highest coordinated atoms for small neutral strontium clusters are the shortest, and therefore the delocalization of valence electrons is more pronounced in the vicinity of such bonds [43]. Examples of such bonds are the short bond between the base atoms in Sr_5; the bond sharing the pyramids in Sr_6, and the bond joining the apex atoms in Sr_7 and Sr_8. A similar behavior has been observed for magnesium clusters [26,29].

It is worth noting that the optimized geometry structures for small neutral strontium and magnesium clusters differ significantly from those obtained for sodium clusters (see, e.g., [25,65,66] and references therein). Thus the optimized

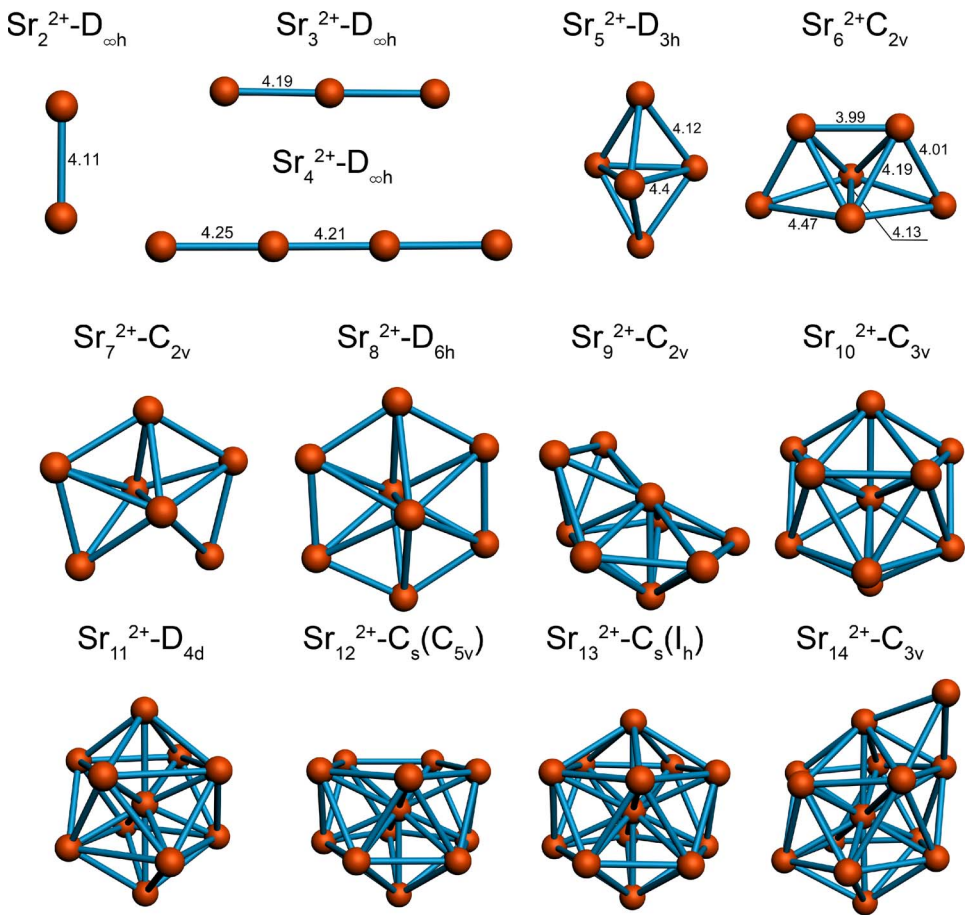

FIG. 3. (Color online) Same as in Fig. 1, but for doubly charged strontium clusters Sr_2^{2+}–Sr_{14}^{2+}.

sodium clusters with $N \leqslant 6$ have the plane structure. For Na_6, both plane and spatial isomers with very close total energies exist. The planar behavior of small sodium clusters has been explained as a result of the successive filling of the 1σ and 1π symmetry orbitals by delocalized valence electrons [65], in accord with the deformed jellium model calculations [22]. The geometry structure of small alkali metal clusters is mainly defined by the closure of electronic shells of the valence electrons. Contrary to the small sodium clusters, the strontium and magnesium clusters are tridimensional already at $N=4$, forming structures nearly the same as the van der Waals bonded clusters. It has been shown that the evolution of the alkaline-earth metal clusters properties is governed by an interplay of the electronic and geometry shell closures [26,30].

In the size region $N \geqslant 9$ the optimized geometry structures for strontium and magnesium clusters become different. Thus the Mg_9 cluster has a structure of tricapped trigonal prism. The formation of the trigonal prism core plays an important role in the magnesium cluster growth process and is closely connected with the future formation of elements of the hexagonal closest-packing (hcp) lattice of the bulk magnesium [26]. For small strontium clusters, however, a motif based on the icosahedral structure dominates the cluster growth. It was shown in Ref. [43] that the icosahedral growth of strontium clusters is induced by the *sp-d* hybridization. Icosahedral growth in the cluster size region $8 \leqslant N \leqslant 13$ results in the successive capping of the pentagonal bipyramid core (structure of the Sr_7 cluster). Thus the Sr_8 cluster is a capped pentagonal bipyramid and Sr_9 has a structure of bicapped pentagonal bipyramid. We have found however that for $N=10$, icosahedral isomer structure is not the lowest-energy one. The most stable structure of Sr_{10} is a tricapped trigonal prism with an additional atom in the center. This structure appears to be new and more bounded compared to those of Refs. [39,42–44]. As we show below, icosahedral growth violation for Sr_{10} is a result of the strong influence of electronic shell effects on structural rearrangements. The configuration of Sr_{11} is a derivative from the structure of Sr_{10}. It can be obtained by addition of an atom to one of the convex quadrangular faces of Sr_{10} and by allowing for relaxation. Starting from Sr_{12} an icosahedral growth mode restores, which leads to a regular icosahedron structure for Sr_{13}. The lowest-energy structure for Sr_{14} is a capped icosahedron.

Figures 2 and 3 show the optimized geometries of singly and doubly charged cationic strontium clusters, respectively. The Sr_2^+ and Sr_2^{2+} cationic dimers are more bound and compact as compared to the neutral dimer. For the singly charged strontium dimer Sr_2^+ the dissociation energy $D_2^+=1.104$ eV and the harmonic vibrational frequency $\omega=75$ cm^{-1} are in good agreement with the experimental values $D_2^+ = 1.092 \pm 0.016$ eV and $\omega = 86 \pm 3$ cm^{-1} reported in Ref. [45].

The ground state geometries of the cationic strontium clusters are not very different from those obtained for neutral

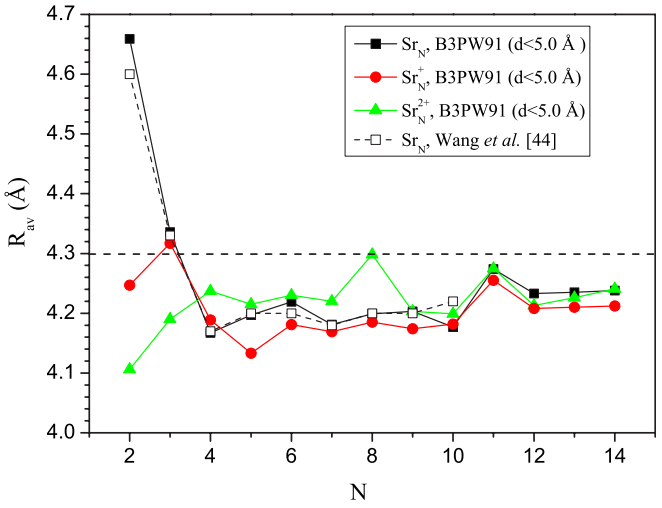

FIG. 4. (Color online) Average bonding distance as a function of cluster size for neutral, singly, and doubly charged strontium clusters. Open squares present the results of the work by Wang *et al.* [44].

parent clusters. Exceptions are observed for small cationic strontium clusters with $N \leqslant 4$, where the equilibrium geometries of Sr_3^+, Sr_3^{2+}, and Sr_4^{2+} are linear chains due to the Coulombic repulsion. A single ionization of the Sr_4 cluster with a structure of a regular tetrahedron T_d lowers its symmetry to D_{2d} for Sr_4^+.

An interesting situation occurs for $N=5$. A single and double ionization of the Sr_5 cluster does not change its D_{3h} symmetry, while changing the cluster's shape. It has already been noticed that the bonds between the highest coordinated atoms for small neutral strontium clusters are the shortest. Thus the bond length between the base atoms of Sr_5 is considerably shorter than that between the base and the apex atoms. Ionization of the Sr_5 cluster leads to a gradual increase in the bond length between the base atoms. Therefore, an elongated triangular bipyramid structure for the Sr_5 isomer transfers to a regular triangular bipyramid structure for Sr_5^+ and finally to an oblate triangular bipyramid structure for Sr_5^{2+}. Single and double ionization of the Sr_7 cluster lowers its point symmetry group from D_{5h} to C_{2v}. Double ionization of the Sr_8 cluster raises its symmetry from C_s to D_{6h} point symmetry group for the Sr_8^{2+} cluster. The formation of a highly symmetric hexagonal bipyramid structure for the Sr_8^{2+} cluster is a result of electronic shell closure. It has already been noticed that closure of electronic shells for Sr_{10} results in violation of icosahedral growth of small neutral strontium clusters. However, charged Sr_{10}^+ and Sr_{10}^{2+} clusters possess opened electronic shells and as a result there is no violation of icosahedral growth. Doubly charged Sr_{11}^{2+} cluster possesses closed electronic shell structure and higher symmetry D_{4d} if compared with the opened shell neutral Sr_{11} cluster (C_{4v}).

In Fig. 4, we present the average bonding distance, R_{av}, calculated within the B3PW91 functional for neutral, singly, and doubly charged Sr clusters. When calculating the average bonding distance in a cluster, interatomic distances smaller than 5.0 Å have only been taken into account. The bulk limit for the strontium fcc lattice [24] is indicated in the figure by a horizontal dashed line.

Figure 4 demonstrates that the dependence of the average bonding distance on cluster size has essentially nonmonotonous oscillatory behavior. For a weakly bounded Sr_2 dimer, the bonding distance is equal to 4.659 Å, which is in good agreement with the experimental result 4.45 Å of Ref. [63].

The appearance of the minima in the size dependence of the average bonding distance shows that Sr_4, Sr_7, and Sr_{10} clusters (8, 14, and 20 valence electrons, respectively) are more tightly packed than their neighbors. This behavior can be interpreted by the influence of electronic shell effects on the geometrical structure of strontium clusters. It supports the conclusion of Ref. [67] that electronic shell effects can enhance the stability of geometric structures resulting from dense ionic packing. Figure 4 demonstrates the good agreement of our results with the dependence of R_{av} on N calculated in [44] for neutral Sr clusters, except for the case of Sr_{10}. It was already noted that the Sr_{10} cluster violates icosahedral growth due to the strong influence of electronic shell effects. Therefore, this structure is more bounded if compared with that of Ref. [44].

Evolution of the average bonding distance with cluster size differs for alkaline-earth clusters from that for clusters of alkali metals. For neutral alkali metal clusters, one can see odd-even oscillations of R_{av} atop its systematic growth and approaching the bulk limit [25]. These features have the quantum origin and arise due to the spin coupling of the delocalized valence electrons. For alkaline-earth metal clusters, the average bonding distance depends on their size nonmonotonically. Such an irregular behavior is induced both by the closure of electronic shells of the delocalized electrons and by the structural rearrangements [26].

Manifestation of the magic numbers in the dependence of the average bonding distance on cluster size coinciding with the deformed jellium model magic numbers does not imply, however, the rapid metallization of strontium clusters. To investigate the transition of van der Waals to metal bonding in strontium clusters it is necessary to explore the evolution of their electronic properties. Below we perform such analysis in detail.

Filled circles and triangles in Fig. 4 represent the average bonding distance as a function of cluster size calculated for singly and doubly charged strontium clusters, respectively.

Figure 4 demonstrates the essential difference in the cluster size dependence of R_{av} for the ionized and neutral strontium clusters with $N \leqslant 8$. The small singly charged strontium clusters are more compact in comparison with the corresponding neutral clusters. For example, for Sr_2^+ the bonding distance is equal to 4.247 Å, which is much less than in the case of Sr_2. This phenomenon has a simple physical explanation: The removed electron is taken from the antibonding orbital. The fact that cationic strontium clusters are more stable than the parent neutral and anionic clusters has already been noted in [26,31]. Within the size range $N \geqslant 7$, the average bonding distances for singly charged and neutral strontium clusters behave similarly. The absolute value of R_{av} for singly charged clusters is slightly smaller in this region of N. Figure 4 demonstrates that singly charged Sr_5^+, Sr_7^+, and Sr_9^+ clusters are more tightly packed than their neighbors. Such an alteration in packing after ionization occurs due to manifestation of electronic shell effects and has already been ob-

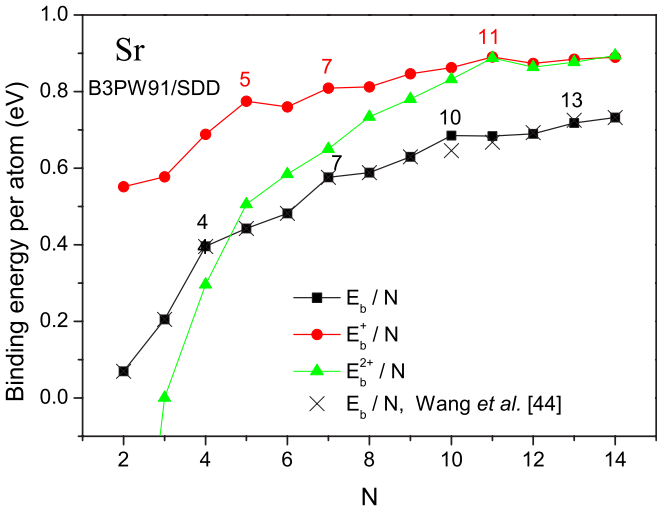

FIG. 5. (Color online) Binding energy per atom for the most stable neutral (filled squares), singly charged (filled circles), and doubly charged (filled triangles) strontium clusters as a function of cluster size. Crosses present the results of the work by Wang *et al.* [44].

served for cationic magnesium [26] and strontium [51] clusters.

Figure 4 shows that small doubly charged Sr_2^{2+} and Sr_3^{2+} clusters are more compact in comparison with the corresponding neutral and singly charged clusters. Thus, for Sr_2^{2+}, the bonding distance is equal to 4.106 Å. However, in the size range $4 \leqslant N \leqslant 10$ doubly charged clusters are less compact. This fact can be explained by the influence of Coulombic repulsion forces on cluster structure. It is known that small doubly charged strontium clusters are metastable within the size range $N \leqslant 7$ and can decay via Coulombic fission if they have enough energy to overcome the fission barrier [51].

B. Binding energy per atom for Sr_N, Sr_N^+, and Sr_N^{2+} clusters

The binding energy per atom for neutral, singly, and doubly charged atomic clusters is defined as follows:

$$E_b/N = E_1 - E_N/N, \tag{1}$$

$$E_b^+/N = [(N-1)E_1 + E_1^+ - E_N^+]/N, \tag{2}$$

$$E_b^{2+}/N = [(N-2)E_1 + 2E_1^+ - E_N^{2+}]/N, \tag{3}$$

where E_N, E_N^+, and E_N^{2+} are the energies of a neutral, singly, and doubly charged N-particle atomic cluster, respectively. E_1 and E_1^+ are the energies of a single atom and an ion.

Figure 5 shows the dependence of the binding energy per atom for the most stable neutral, singly, and doubly charged Sr clusters as a function of cluster size. Filled squares, circles, and triangles represent binding energies E_b/N, E_b^+/N, and E_b^{2+}/N obtained within the B3PW91/SDD method. The corresponding point symmetry groups and the accurate values of the total energies calculated within the B3PW91/SDD approximation for the most stable neutral, singly, and doubly charged clusters as well as their isomers are presented in Tables I–III, respectively. Crosses in Fig. 5 present the results of the work by Wang *et al.* [44].

TABLE I. Total energies and the point symmetry groups for a variety of isomers of neutral strontium clusters. Calculations have been done by the B3PW91/SDD method.

N	Point group	Energy (a.u.)	N	Point group	Energy (a.u.)
1		**−30.70847**	8	**C_s**	**−245.84074**
2	**$D_{\infty h}$**	**−61.42205**		C_{2v}	−245.82452
3	**D_{3h}**	**−92.14800**		T_d	−245.82432
	$D_{\infty h}$	−92.13653		C_{2v}	**−245.82417**
4	**T_d**	**−122.89206**		$D_{\infty h}$	**−276.42527**
	D_{2h}	**−122.87073**	9	**C_{2v}**	**−276.58446**
	C_{2v}	−122.86321		C_s	−276.57496
	$D_{\infty h}$	−122.85123		C_{2v}	−276.57416
	D_{4h}	−122.83811		D_{3h}	−276.56851
5	**D_{3h}**	**−153.62367**		C_{3v}	−276.56442
	C_{3v}	−153.60733		D_{9h}	−276.43620
	C_{2v}	−153.59587		$D_{\infty h}$	−276.42527
	D_{2d}	−153.58852	10	**D_{3h}**	**−307.33650**
	D_{2h}	−153.58822		C_{4v}	−307.33647
	D_{5h}	−153.57875		D_{3h}	−307.33584
	$D_{\infty h}$	−153.56600		C_1	−307.31907
	D_{4h}	−153.55701		C_{3v}	−307.31242
6	C_{2v}	**−184.35712**		T_d	−307.30354
	D_{2h}	−184.35228		C_{2v}	−307.29648
	C_s	−184.34533		D_{4d}	−307.29497
	D_{4h}	−184.34482	11	**C_{4v}**	**−338.06968**
	C_{5v}	−184.33493		C_s	−338.06433
	D_{4h}	−184.33275		C_s	−338.06289
	D_{4h}	−184.32647		C_{3v}	−338.06261
	D_{5h}	−184.32514		C_1	−338.05926
	D_{6h}	−184.28641	12	**C_{5v}**	**−368.80586**
	$D_{\infty h}$	−184.28081		C_1	−368.79762
7	**D_{5h}**	**−215.10755**	13	**I_h**	**−399.55317**
	C_{3v}	−215.09144		C_s	−399.54227
	C_s	−215.08857		C_{2v}	−399.53176
	C_{3v}	−215.06345	14	**C_{3v}**	**−430.29538**
	C_{3d}	−215.05850		C_s	−430.28818
	D_{3h}	−215.05488		C_{2v}	−430.28723
	$D_{\infty h}$	−214.99562		C_{2v}	−430.26811

For small Sr clusters the binding energy per atom increases steadily with the cluster size. The peculiarity in the size dependence of E_b/N, at N=4, 7, and 10 correspond to the most stable configurations of neutral Sr clusters. The same magic numbers have also been obtained from the analysis of binding energies of small neutral Mg [26] clusters.

The analysis of the second differences of the binding energy, $\Delta^2 E_N = E_{N+1} - 2E_N + E_{N-1}$, points to a relative stability of the Sr_{13} cluster, in addition to the magic clusters Sr_4, Sr_7, and Sr_{10} (see Fig. 6). The principal magic numbers 7 and 13 can

TABLE II. Total energies and the point symmetry groups for a variety of isomers of singly charged strontium clusters. Calculations have been done by the B3PW91/SDD method.

N	Point group	Energy (a.u.)	N	Point group	Energy (a.u.)
1		**−30.50178**		C_s	−214.94678
2	$D_{\infty h}$	**−61.25080**		C_s	−214.94521
3	$D_{\infty h}$	**−91.98237**		C_s	−214.94128
	C_{2v}	−91.98166		C_{6v}	−214.92417
	C_{2v}	−91.98114		D_{3h}	−214.92301
4	$\mathbf{D_{2d}}$	**−122.72840**		D_{6h}	−214.92288
	D_{2h}	−122.72200		$D_{\infty h}$	−214.86911
	C_{2v}	−122.71088	8	$\mathbf{C_s}$	**−245.69976**
	D_{4h}	−122.71024	9	$\mathbf{C_{2v}}$	**−276.44939**
	$D_{\infty h}$	−122.70764		C_{2v}	−276.43578
5	$\mathbf{D_{3h}}$	**−153.47798**		C_s	−276.42626
	C_{4v}	−153.46502		$D_{\infty h}$	−276.30501
	C_{2v}	−153.44398	10	$\mathbf{C_{3v}}$	**−307.19508**
	C_{2v}	−153.43894		C_s	−307.18589
	$D_{\infty h}$	−153.42975		C_{3v}	−307.16873
	D_{2h}	−153.42803	11	$\mathbf{D_{4d}}$	**−337.94355**
	D_{5h}	−153.38024		C_s	−337.94355
6	$\mathbf{C_{2v}}$	**−184.21175**		C_{3v}	−337.93088
	C_{2v}	−184.20765		C_{3v}	−337.92971
	D_{2h}	−184.19720		C_1	−337.92839
	D_{4h}	−184.18385		C_s	−337.92753
	C_{2v}	−184.16255	12	$\mathbf{C_s}$	**−368.68015**
	$D_{\infty h}$	−184.15003	13	$\mathbf{I_h}$	**−399.42589**
7	$\mathbf{C_{2v}}$	**−214.96077**		D_{5d}	−399.42566
	C_{2v}	−214.96077	14	$\mathbf{C_{3v}}$	**−430.16961**
	D_{5h}	−214.96050		C_{3v}	−430.15400

TABLE III. Total energies and the point symmetry groups for a variety of isomers of doubly charged strontium clusters. Calculations have been done by the B3PW91/SDD method.

N	Point group	Energy (a.u.)	N	Point group	Energy (a.u.)
1		**−30.09466**		C_s	−214.70161
2	$\mathbf{D_{\infty h}}$	**−60.93737**		$D_{\infty h}$	−214.66885
3	$\mathbf{D_{\infty h}}$	**−91.71211**	8	$\mathbf{D_{6h}}$	**−245.47031**
	C_{2v}	−91.68897	9	$\mathbf{C_{2v}}$	**−276.22101**
4	$\mathbf{D_{\infty h}}$	**−122.46405**		C_{2v}	−276.21198
	D_{2h}	−122.46174		C_s	−276.20961
	D_{4h}	−122.46080		D_{3h}	−276.15813
	D_{3h}	−122.45971		$D_{\infty h}$	−276.12063
5	$\mathbf{D_{3h}}$	**−153.22187**		C_{2v}	−276.10672
	C_{4v}	−153.21640	10	$\mathbf{C_{3v}}$	**−306.97717**
	C_{2v}	−153.20566		C_{2v}	−306.97017
	$D_{\infty h}$	−153.20478		C_{2v}	−306.97007
	C_{3v}	−153.19623		C_s	−306.97694
	D_{2h}	−153.16818		C_s	−306.96509
	D_{5h}	−153.14856		C_{2v}	−306.93038
6	$\mathbf{C_{2v}}$	**−183.96634**		C_{4v}	−306.91598
	D_{4h}	−183.95722	11	$\mathbf{D_{4d}}$	**−337.73861**
	D_{4h}	−183.95044		C_s	−337.73773
	O_h	−183.94618		C_s	−337.72032
	C_{2v}	−183.94147		C_s	−337.71191
	D_{6h}	−183.93625		C_s	−337.71174
	$D_{\infty h}$	−183.93894		C_1	−337.71162
	D_{4h}	−183.93852	12	$\mathbf{C_s}$	**−368.46909**
7	$\mathbf{C_{2v}}$	**−214.71314**	13	$\mathbf{C_s}$	**−399.21551**
	C_{2v}	−214.71228		C_s	−399.21547
	D_{5h}	−214.71005	14	$\mathbf{C_{3v}}$	**−429.96531**
	C_s	−214.70977		C_s	−429.96361
	D_{6h}	−214.70406		C_{2v}	−429.95582
	D_{3h}	−214.70311			

be explained by atomic shell closing effects. Indeed, the enhanced stability of Sr_7 and Sr_{13} clusters arises when their ionic structure is highly symmetric and corresponds to the icosahedral type of packing. This icosahedral growth sequence for metal clusters has also been seen for clusters of Ba [68], which exhibit nonmetal to metal transition with increasing cluster size. It is important to note that for alkaline-earth metal clusters there is a strong competition between geometrical and electronic shell closures [26,51]. The electronic configuration of the Sr atom is $[Kr]5s^2$, which means that there are two valence electrons per atom. Accounting for the semicore $4p$ electrons of strontium increases the absolute value of the binding energy by about 10–20% although it does not change the general qualitative trend in the evolution of properties of small strontium clusters [43]. The most stable magic clusters Sr_4, Sr_7, and Sr_{10} possess $N_{el}=8$, 14, and 20 valence electrons, respectively, which is in agreement with the deformed jellium model (see, e.g. [20–23] and references therein as well as discussions in [26,51]).

Filled circles in Fig. 5 show the binding energy for singly charged strontium clusters. The singly charged small strontium clusters are more stable towards decay in comparison with neutral clusters. This phenomenon has a simple physical explanation: The removed electron is taken from the antibonding orbital, and thus small cationic strontium clusters are bounded stronger. A similar effect has been discussed for cationic magnesium clusters in [26].

The local maxima in the size dependence of the binding energy E_b^+/N for the Sr_5^+, Sr_7^+, and Sr_{11}^+ clusters indicate their enhanced stability. This result is in very good agreement with the experimental data on cation clusters, which show 5, 7, and 11 to be magic numbers [46]. The analysis of the second differences of the binding energy (see Fig. 6) also suggests relative stability of the Sr_9^+ and Sr_{13}^+ clusters.

Figures 5 and 6 clearly demonstrate that the single ionization of small strontium clusters results in alteration of the "electronic" magic numbers. The similar change of the magic number from $N=4$ for neutral to $N=5$ for cationic magnesium clusters has been noticed in our recent work [26]. This fact can be explained by the manifestation of shell effects. The singly charged alkaline-earth metal clusters always possess an odd number of valence electrons and, thus, always contain open electronic shells. In this case the en-

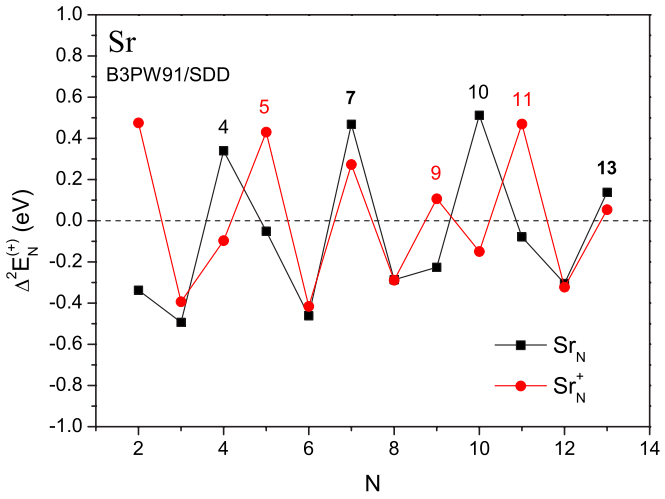

FIG. 6. (Color online) Second differences of total energy for neutral (filled squares), $\Delta^2 E_N = E_{N+1} - 2E_N + E_{N-1}$, and singly charged (filled circles), $\Delta^2 E_N^+ = E_{N+1}^+ - 2E_N^+ + E_{N-1}^+$, strontium clusters.

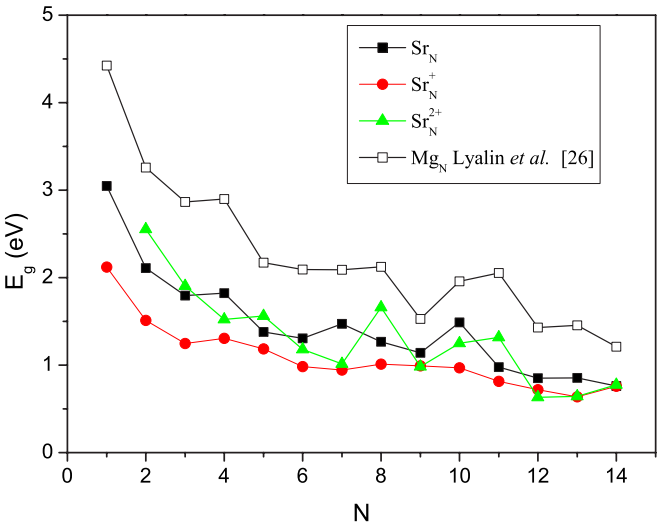

FIG. 7. (Color online) Gap between the highest occupied and the lowest unoccupied eigenstates (HOMO-LUMO gap) for neutral, singly, and doubly charged strontium clusters as a function of cluster size. Open squares represent the HOMO-LUMO gap calculated for Mg clusters [26].

hanced stability of a singly charged alkaline-earth metal cluster ion arises, when the electronic configuration of the ion has one hole in or an extra electron above the filled shells [26]. Thus the electronic configuration containing an extra electron becomes more favorable for Sr_5^+ and Sr_{11}^+. Note that magic numbers $N=7$ and 13 correspond to the geometry shell closures, and therefore they do not alter due to single ionization. This effect is clearly seen in Fig. 6.

Filled triangles in Fig. 5 present the binding energy per atom, E_b^{2+}/N, for the doubly charged strontium clusters. Figure 5 demonstrates the fast increase in the value of E_b^{2+}/N with the cluster size. Binding energy E_b^{2+}/N possesses a negative value for Sr_2^{2+}, and is negligible for Sr_3^{2+}. This fact means that Sr_2^{2+} and Sr_3^{2+} clusters are intrinsically unstable towards complete fragmentation, because the final state of the system is energetically more favorable in comparison with the initial state of the parent cluster. However, in order to decay the parent cluster has to overcome the Coulombic fission barrier. The doubly charged strontium clusters remain metastable for $N \leqslant 7$ [51]. For larger sizes $N \geqslant 8$ doubly charged strontium clusters are intrinsically stable towards the Coulombic fission. Therefore, the critical *appearance* size for the doubly charged strontium clusters is equal to $N_{\mathrm{app}} = 8$ [51]. It is important to note that we found a drastic alteration of the cluster geometry upon ionization for $N=8$. The effect of alteration of the ionic structure for Sr_8^{2+} arises due to the influence of the electronic shell effects on the cluster geometry. It is very important to take into account such an alteration when calculating the critical size of stability of doubly charged strontium clusters.

C. HOMO-LUMO gap and electronic structure

Let us now consider how the gap E_g between the highest occupied and the lowest unoccupied molecular orbitals (HOMO-LUMO gap) for Sr clusters evolves with increasing cluster size. The HOMO-LUMO gap can be used to analyze the transition to metallicity with increasing cluster size. Figure 7 shows the HOMO-LUMO gap for neutral, singly, and doubly charged strontium clusters as a function of N. We also compare our results with those presented in Ref. [26] for Mg clusters.

The gap E_g calculated for neutral strontium clusters shows the oscillatory behavior accompanied by the gradual decrease in the absolute value. Maxima in this dependence at $N=4$, 7, 10, and 13 correspond to the most stable magic clusters. It was discussed before that the most stable magic clusters Sr_4, Sr_7, and Sr_{10} possess $N_{\mathrm{el}}=8$, 14, and 20 valence electrons, respectively, which is in accordance with the deformed jellium model. In addition to the electronic shell closure for $N=4$, 7, and 10, clusters Sr_7 and Sr_{13} possess closed geometry shells. Thus variations of E_g both appear due to the electronic subshell closures and the cluster structural rearrangements. Similar behavior of E_g as a function of N has been noticed for Mg clusters [26] (see Fig. 7). It is important to mention that the size dependence of E_g for neutral Sr clusters differs from that for Na clusters. For neutral sodium clusters E_g has an odd-even oscillatory behavior as a function of N with local maxima at $N=6$, 8, 10, 14, and 20. These maxima correspond to the electronic shell closures as predicted by the deformed jellium model.

Figure 7 shows that the HOMO-LUMO gap calculated for singly charged strontium clusters demonstrates a rather smooth decrease in the absolute value. The singly charged strontium clusters always possess an odd number of valence electrons; therefore, electronic shell effects in such systems are quenched. For doubly charged strontium clusters the gap E_g demonstrates the oscillatory behavior with pronounced maxima at $N=5$, 8, and 11. The corresponding clusters Sr_5^{2+}, Sr_8^{2+}, and Sr_{11}^{2+} possess $N_{\mathrm{el}}=8$, 14, and 20 valence electrons, respectively, in full agreement with the deformed jellium model. We note that the HOMO-LUMO gap for strontium clusters remains rather large in all ranges of considered sizes N. This fact confirms the conclusion on the slow and non-

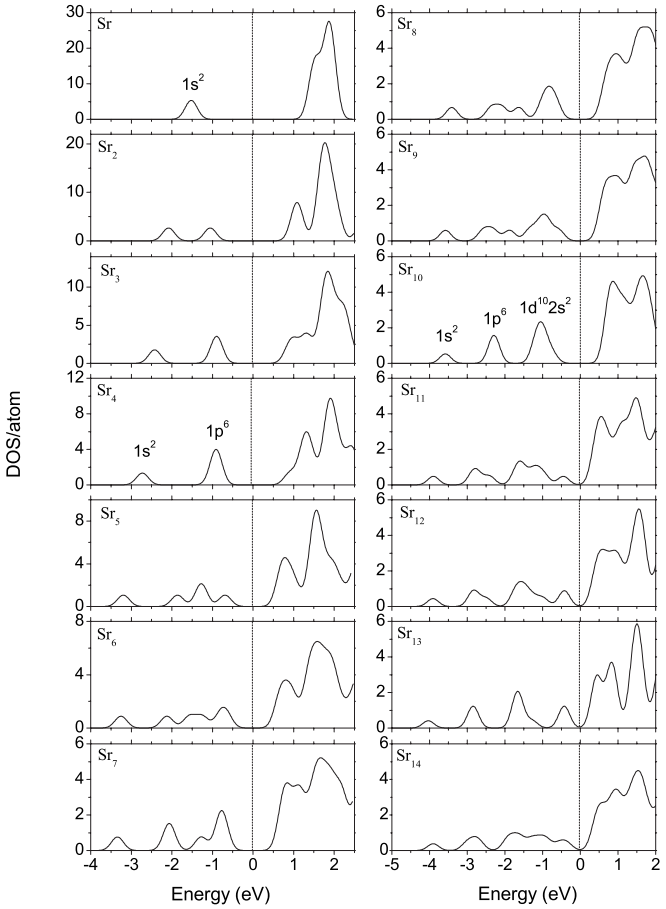

FIG. 8. Density of states for neutral strontium clusters. Gaussian broadening of half-width 0.15 eV has been used. The zero level of energy is chosen equal to the Fermi level E_f (vertical line).

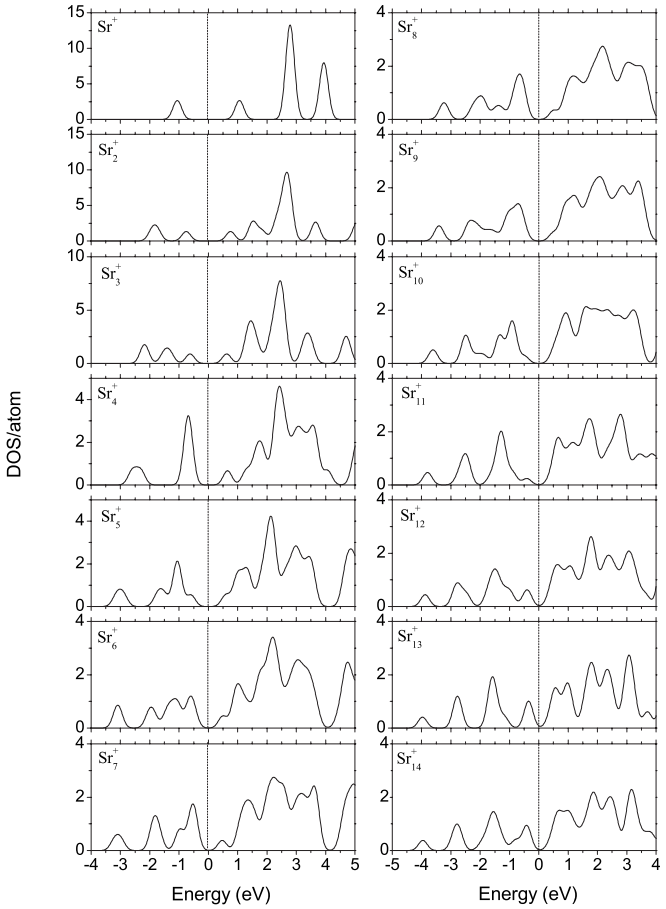

FIG. 9. Same as in Fig. 8, but for singly charged strontium clusters.

monotonous evolution of metallic properties in Sr clusters.

Figures 8–10 demonstrate the evolution of the density of electronic states (DOS) for neutral, singly, and doubly charged strontium clusters, respectively. For the sake of comparison, for each spectrum the zero level of energy is chosen equal to the Fermi level E_f of the corresponding cluster. For the strontium atom, the energy level of 5*s* valence electron lays at 1.52 eV below the Fermi level, while unoccupied 5*p* and 4*d* levels lay at 1.52 eV and 1.89 eV above the Fermi level, respectively. For the dimer Sr_2 valence electrons form one bonding and one antibonding σ orbital. The HOMO-LUMO gap is relatively high (2.11 eV); therefore, there is no interaction of valence electrons with the 4*d* and 5*p* states. Figure 8 clearly demonstrates formation of the electronic shell structure of small strontium clusters in accord with the jellium model. Sharp peaks in the energy spectrum of Sr_4 and Sr_{10} correspond to the closed electronic shells $1s^21p^6$ and $1s^21p^61d^{10}2s^2$, respectively. The DOS spectra for small neutral strontium clusters are in good agreement with the results of Ref. [43] with the exception of Sr_{10}.

As we discussed above, we found that the most stable Sr_{10} structure violates icosahedral growth and it is more bounded compared to those of Refs. [42–44]. The icosahedral growth violation for Sr_{10} is a result of the strong influence of electronic shell effects on structural rearrangements. It is seen from Fig. 8 that the DOS spectrum for Sr_{10} cluster contains well separated maxima below the Fermi level. These maxima correspond to the closed electronic shells $1s^21p^61d^{10}2s^2$.

As cluster size increases, the HOMO-LUMO gap decreases, the unoccupied 5*p* and 4*d* states are shifting to the higher binding energy, while the highest occupied molecular orbital shifts toward the lower binding energy. This results in an increase in interaction between valence and unoccupied states and, hence, an increase in *sp-d* hybridization. In turn, the *sp-d* hybridization significantly changes electronic states near the HOMO level. The most stable clusters possess local maxima in the size dependence of the HOMO-LUMO gap and therefore for such clusters *sp-d* hybridization decreases. Therefore, the electronic states of magic clusters are similar to those expected from a jellium model as can be seen from Fig. 8.

For the charged strontium clusters the DOS spectra of low-lying valence states are quite similar to those obtained for the neutral clusters. The difference can be observed for the states near the HOMO as well as for the unoccupied states. Single and double ionization of the strontium dimer leads to removing valence electrons from the antibonding HOMO orbital that can be seen in Figs. 9 and 10. Removing the electron from the antibonding orbital results in increased stability of Sr_2^+ and Sr_2^{2+} ions. The most stable configuration of Sr_3^+, Sr_3^{2+}, and Sr_4^{2+} is a linear chain. For the linear geom-

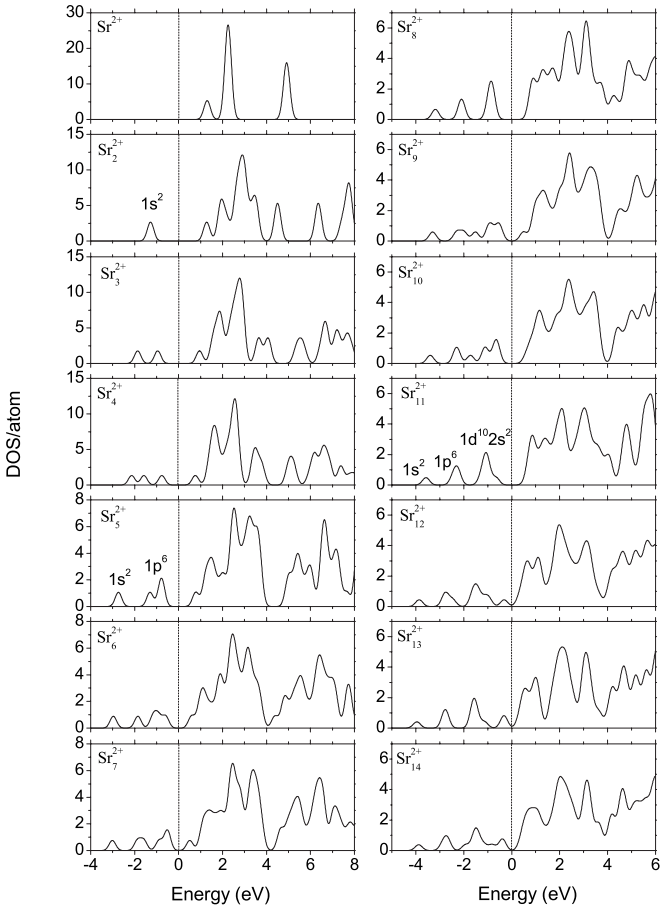

FIG. 10. Same as in Fig. 8, but for doubly charged strontium clusters.

etry the successive filling of σ orbitals is more favorable energetically. It is seen from Figs. 9 and 10 that this fact has an affect on the DOS spectra of Sr_3^+, Sr_3^{2+}, and Sr_4^{2+} clusters. As we discussed above, the ionization of the Sr_{10} magic cluster results in alteration of the magic number from 10 to 11 due to the electronic shell effects. Figure 10 confirms the conclusion about the origin of such an alteration. Indeed, energetically well separated maxima below the Fermi level correspond to the closed electronic configuration $1s^2 1p^6 1d^{10} 2s^2$ of the Sr_{11}^{2+} cluster. In conclusion it is necessary to note that DOS spectra of free electronic states obtained for cationic clusters are more complicated if compared with those calculated for neutral clusters due to the additional Coulombic field.

The DOS spectra are very sensitive to the cluster isomer structure, and thus can be used for determination of the geometry of strontium clusters. Recently, a similar approach has been used for identification of a specific icosahedral growth motif of medium-sized sodium clusters [69]. Figure 11 presents the DOS spectra calculated for three different isomers of I_h, C_s, and C_{2v} point symmetry group of the Sr_{13} cluster. The energies of the two lowest lying states are not affected by the cluster geometry alterations. These states can be associated with the $1s^2$ and $1p^6$ levels in accord with the spherical jellium model. However, from Fig. 11 one can see considerable rearrangement and splitting of the states lying

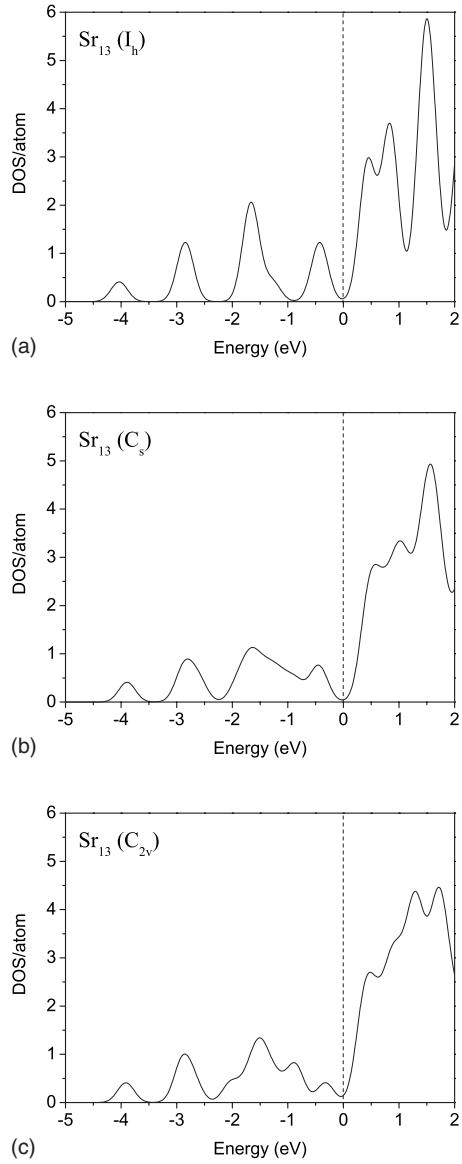

FIG. 11. Density of states for three different isomers of Sr_{13}. From left to right: Isomers of I_h, C_s, and C_{2v} point symmetry groups, respectively. Gaussian broadening of half-width 0.15 eV has been used. The zero level of energy is chosen equal to the Fermi level E_f (vertical line).

in the vicinity and above the Fermi level. The level splitting due to the geometry distortion of the cluster has been explored in detail in Refs. [20–22] within the deformed jellium model. A similar behavior of energy levels is well known for deformed nuclei (see [70]).

IV. CONCLUSION

The optimized structures and electronic properties of neutral, singly, and doubly charged strontium clusters have been investigated using *ab initio* theoretical methods based on density-functional theory. We have systematically calculated the optimized geometries of neutral, singly, and doubly charged strontium clusters consisting of up to 14 atoms, av-

erage bonding distances, electronic shell closures, binding energies per atom, the gap between the highest occupied and the lowest unoccupied molecular orbitals, and spectra of the electronic density of states. We have shown that the size evolution of structural and electronic properties of strontium clusters is governed by an interplay of the electronic and geometry shell closures. The influence of the electronic shell effects on structural rearrangements can lead to violation of the icosahedral growth motif of strontium clusters. We have demonstrated that electronic shell structure of small strontium clusters forms in accord with the jellium model. It is shown that the excessive charge essentially affects the optimized geometry of strontium clusters. Ionization of small strontium clusters results in the alteration of the magic numbers. We demonstrate that the strong dependence of the DOS spectra on details of ionic structure allows one to perform a reliable identification of the geometry of the strontium clusters.

ACKNOWLEDGMENTS

This work is partially supported by the European Commission within the Network of Excellence project EXCELL, and by INTAS under Grant No. 03-51-6170. The authors gratefully acknowledge support by the Frankfurt Center for Scientific Computing.

[1] W. A. de Heer, Rev. Mod. Phys. **65**, 611 (1993).
[2] M. Brack, Rev. Mod. Phys. **65**, 677 (1993).
[3] C. Bréchignac and J. P. Connerade, J. Phys. B **27**, 3795 (1994).
[4] *Clusters of Atoms and Molecules, Theory, Experiment and Clusters of Atoms*, edited by H. Haberland, Springer Series in Chemical Physics Vol. 52 (Springer, Berlin, 1994).
[5] U. Näher, S. Bjørnholm, S. Frauendorf, F. Garcias, and C. Guet, Phys. Rep. **285**, 245 (1997).
[6] *Metal Clusters*, edited by W. Ekardt (Wiley, New York, 1999).
[7] *Atomic Clusters and Nanoparticles*, NATO Advanced Study Institute, Les Houches Session LXXIII, Les Houches, 2000, edited by C. Guet, P. Hobza, F. Spiegelman, and F. David (EDP Sciences and Springer-Verlag, Berlin, 2001).
[8] *Theory of Atomic and Molecular Clusters. With a Glimpse at Experiments*, edited by J. Jellinek, Springer Series in Cluster Physics (Springer, Berlin, 1999).
[9] *Metal Clusters at Surfaces. Structure, Quantum Properties, Physical Chemistry*, edited by K.-H. Meiwes-Broer, Springer Series in Cluster Physics (Springer, Berlin, 1999).
[10] *Latest Advances in Atomic Cluster Collisions: Fission, Fusion, Electron, Ion and Photon Impact*, edited by J.-P. Connerade and A. V. Solov'yov (Imperial College Press, London, 2004).
[11] F. Baletto and R. Ferrando, Rev. Mod. Phys. **77**, 371 (2005).
[12] J. A. Alonso, *Structure and Properties of Atomic Nanoclusters* (Imperial College Press, London, 2005).
[13] W. D. Knight, K. Clemenger, W. A. de Heer, W. A. Saunders, M. Y. Chou, and M. L. Cohen, Phys. Rev. Lett. **52**, 2141 (1984).
[14] J. M. Eisenberg and W. Greiner, *Nuclear Theory. Vol. 1. Collective and Particle Models* (North-Holland, Amsterdam, 1985).
[15] W. Ekardt, Phys. Rev. B **29**, 1558 (1984).
[16] W. Ekardt, Phys. Rev. B **32**, 1961 (1985).
[17] W. Ekardt and Z. Penzar, Phys. Rev. B **38**, 4273 (1988).
[18] W. Ekardt and Z. Penzar, Phys. Rev. B **43**, 1322 (1991).
[19] B. Montag, Th. Hirschmann, J. Meyer, P.-G. Reinhard, and M. Brack, Phys. Rev. B **52**, 4775 (1995).
[20] A. G. Lyalin, S. K. Semenov, A. V. Solov'yov, N. A. Cherepkov, and W. Greiner, J. Phys. B **33**, 3653 (2000).
[21] A. G. Lyalin, S. K. Semenov, A. V. Solov'yov, N. A. Cherepkov, J.-P. Connerade, and W. Greiner, J. Chin. Chem. Soc. (Taipei) **48**, 419 (2001).
[22] A. Matveentzev, A. Lyalin, I. A. Solov'yov, A. V. Solov'yov, and W. Greiner, Int. J. Mod. Phys. E **12**, 81 (2003).
[23] A. G. Lyalin, A. Matveentzev, I. A. Solov'yov, A. V. Solov'yov, and W. Greiner, Eur. Phys. J. D **24**, 15 (2003).
[24] N. W. Ashcroft and N. D. Mermin, *Solid State Physics* (Saunders College Publishing, New York, 1976).
[25] I. A. Solov'yov, A. V. Solov'yov, and W. Greiner, Phys. Rev. A **65**, 053203 (2002).
[26] A. Lyalin, I. A. Solov'yov, A. V. Solov'yov, and W. Greiner, Phys. Rev. A **67**, 063203 (2003).
[27] P. H. Acioli and J. Jellinek, Phys. Rev. Lett. **89**, 213402 (2002).
[28] J. Jellinek and P. H. Acioli, J. Phys. Chem. A **106**, 10919 (2002).
[29] V. Kumar and R. Car, Phys. Rev. B **44**, 8243 (1991).
[30] J. Akola, K. Rytkönen, and M. Manninen, Eur. Phys. J. D **16**, 21 (2001).
[31] F. Reuse, S. N. Khanna, V. de Coulon, and J. Buttet, Phys. Rev. B **41**, 11743 (1990).
[32] F. Reuse, S. N. Khanna, V. de Coulon, and J. Buttet, Phys. Rev. B **39**, 12911 (1989).
[33] P. Delaly, P. Ballone, and J. Buttet, Phys. Rev. B **45**, 3838 (1992).
[34] G. Durand, J. Chem. Phys. **91**, 6225 (1989).
[35] S. N. Khanna, F. Reuse, and J. Buttet, Phys. Rev. Lett. **61**, 535 (1988).
[36] Li. Serra, P.-G. Reinhard, and E. Suraud, Eur. Phys. J. D **18**, 327 (2002).
[37] Th. Diederich, T. Döppner, J. Braune, J. Tiggesbäumker, and K.-H. Meiwes-Broer, Phys. Rev. Lett. **86**, 4807 (2001).
[38] O. C. Thomas, W. Zheng, S. Xu, and K. H. Bowen, Phys. Rev. Lett. **89**, 213403 (2002).
[39] J. E. Hearn and R. L. Johnston, J. Chem. Phys. **107**, 4674 (1997).
[40] J. P. K. Doye and D. J. Wales, J. Chem. Soc., Faraday Trans. **93**, 4233 (1997).
[41] R. O. Jones, J. Chem. Phys. **71**, 1300 (1979).
[42] Y. Wang, H.-J. Flad, and M. Dolg, J. Phys. Chem. A **104**, 5558 (2000).
[43] V. Kumar and Y. Kawazoe, Phys. Rev. B **63**, 075410 (2001).
[44] G. M. Wang, E. Blaisten-Barojas, A. E. Roitberg, and T. P.

Martin, J. Chem. Phys. **115**, 3640 (2001).
[45] Ph. Dugourd, J. Chevaleyre, C. Bordas, and M. Broyer, Chem. Phys. Lett. **193**, 539 (1992).
[46] C. Bréchignac, Ph. Cahuzac, N. Kébaïli, J. Leygnier, and H. Yoshida, Phys. Rev. B **61**, 7280 (2000).
[47] M. Heinebrodt, S. Frank, N. Malinowski, F. Tast, I. M. L. Billas, and T. P. Martin, Z. Phys. D: At., Mol. Clusters **40**, 334 (1997).
[48] C. Bréchignac, Ph. Cahuzac, N. Kébaïli, and J. Leygnier, Phys. Rev. Lett. **81**, 4612 (1998).
[49] C. Bréchignac, Ph. Cahuzac, B. Concina, and J. Leygnier, Phys. Rev. Lett. **89**, 203401 (2002).
[50] C. Bréchignac, Ph. Cahuzac, B. Concina, and J. Leygnier, Phys. Rev. Lett. **92**, 083401 (2004).
[51] A. Lyalin, A. V. Solov'yov, C. Bréchignac, and W. Greiner, J. Phys. B **38**, L129 (2005).
[52] James B. Foresman and Æleen Frisch, *Exploring Chemistry with Electronic Structure Methods* (Gaussian Inc., Pittsburgh, PA, 1996).
[53] A. D. Becke, Phys. Rev. A **38**, 3098 (1988).
[54] J. P. Perdew, in *Electronic Structure of Solids'91*, edited by P. Ziesche and H. Eschrig (Akademie Verlag, Berlin, 1991), p. 11.
[55] K. Burke, J. P. Perdew, and Y. Wang, in *Electronic Density Functional Theory: Recent Progress and New Directions*, edited by J. F. Dobson, G. Vignale, and M. P. Das (Plenum, New York, 1998).
[56] A. Koshelev, A. Shutovich, I. A. Solov'yov, A. V. Solov'yov, and W. Greiner, Phys. Rev. Lett. **90**, 053401 (2003).
[57] I. A. Solov'yov, A. V. Solov'yov, and W. Greiner, Int. J. Mod. Phys. E **13**, 697 (2004).
[58] O. I. Obolensky, I. A. Solov'yov, A. V. Solov'yov, and W. Greiner, Computing Letters (CoLe) **1**, 313 (2005).
[59] A. Lyalin, A. V. Solov'yov, and W. Greiner, Phys. Rev. A **74**, 043201 (2006).
[60] D. E. Goldberg, *Genetic Algorithms in Search, Optimization, and Machine Learning* (Addison-Wesley, Reading, MA, 1989).
[61] Z. Michalewicz, *Genetic Algorithms+Data Structures =Evolution Programs*, 3rd ed. (Springer, Berlin, Heidelberg, New York, 1996).
[62] M. J. Frisch *et al.*, computer code GAUSSIAN 03, Rev. C. 02 (Gaussian Inc., Pittsburgh, PA, 2004).
[63] G. Gerber, R. Möller, and H. Schneider, J. Chem. Phys. **81**, 1538 (1984).
[64] A. Köhn, F. Weigend, and R. Ahlrichs, Phys. Chem. Chem. Phys. **3**, 711 (2001).
[65] J. L. Martins, J. Buttet, and R. Car, Phys. Rev. B **31**, 1804 (1985).
[66] V. Bonačić-Koutecký, P. Fantucci, and J. Koutecký, Phys. Rev. B **37**, 4369 (1988).
[67] S. M. Reimann, M. Koskinen, H. Häkkinen, P. E. Lindelof, and M. Manninen, Phys. Rev. B **56**, 12147 (1997).
[68] D. Rayane, P. Melinon, B. Cabaud, A. Hoareau, B. Tribollet, and M. Broyer, Phys. Rev. A **39**, 6056 (1989).
[69] O. Kostko, B. Huber, M. Moseler, and B. von Issendorff, Phys. Rev. Lett. **98**, 043401 (2007).
[70] A. B. Migdal, *Qualitative Methods of Quantum Mechanics* (Nauka, Moscow, 1978).